17th Symposium IMEKO TC 4, 3rd Symposium IMEKO TC 19 and 15th IWADC Workshop
Instrumentation for the ICT Era
Sept. 8-10, 2010, Kosice, Slovakia

Experimental Analysis of Shielding Performance in Rail-Launcher Environment

Mirko Marracci[1], Bernardo Tellini[1]

[1] *Department of Electrical Systems and Automation – University of Pisa, Largo Lucio Lazzarino 1, I-56122 Pisa, Italy, phone: +39 0502217300, fax: +39 0502217333, e-mail: bernardo.tellini@ing.unipi.it)*

Abstract- In this paper we develop an experimental analysis aimed at characterizing the shielding performance of shields operating in electromagnetic rail launchers. The experimental analysis is carried out for various shield configurations and different materials. In particular, cylindrical shell cylinders are adopted. The experiments are performed on a rail launcher prototype supplied by a high pulsed power device. Finally, we make some remarks on the measurement of the shielding effectiveness in such critical environments.

I. Introduction

As known from the Schelkunoff's theory, the shielding of low-frequency, low-impedance and high-intensity electromagnetic waves is a complex task [1]. Low-impedance waves reduce the reflection losses, while absorption losses diminish with frequency. Highly permeable materials usually increase the shielding of magnetic fields as a result of the combined flux shunting and flux redirection effects [2], [3]. On the other hand, strong magnetic fields can drastically reduce the shielding performance of magnetic materials as a result of saturation effects. The rail launchers can exhibit magnetic fields up to 20 T in the barrel and this leads to reapproach the concept of shielding as well as of the shielding effectiveness (SE) measurement. Some authors discussed the idea of multi-layered shields [4], [5], showing that the SE increases when the shield is an alternate structure of highly conducting and highly magnetically permeable layers [6], [7]. Another approach uses active shields connected to an external power [8]. In a previous paper, one of the authors developed a numerical study focusing on cylindrical- and disk-shaped shields. In the same paper, some remarks on how to compare the SE of different shield configurations from the "victim point view" were reported [9].
In this paper, we present the results of an experimental analysis aimed at showing the SE for various shield geometries and configurations during shots under different operating conditions. We develop static experiments with no motion of the solid armature. We describe the experimental setup and the adopted operating conditions. Experimental results will be presented in the final version of the paper.

II. Experimental Setup

A 50 kJ supply source is made by a capacitor bank of about 765 μF chargeable up to 10 kV. The source module supplies a rail launcher prototype through a power coaxial connecting cable of about 10 m length. The characteristic parameters of the coaxial cable have been calculated through the use of the Bessel functions to take into account possible skin effects. Results provided an estimated cable resistance R_C of about 7.6 mΩ and a cable inductance L_C of about 1.9 μH. The discharge circuit determines an under damped behaviour during the first part of the transient, while a crowbar diode in parallel to the capacitor prevents from oscillation and causes an exponential decay after the capacitor voltage reaches zero. The time constant of the measured exponential decay is in agreement with the estimated parameters.
In Fig. 1, we show a schematic of the adopted prototype. The rails are 1.5 m long aluminium bars with thickness of 2.5 mm and width of 50 mm. They are separated 50 mm one from the other and they are hold in still position by a series of properly mounted clamps. Solid armatures are made by 50 mm long aluminium rods, while plasma armature is formed by ablating thin copper wires or thin aluminium tapes. A photograph of the rails is shown in Fig. 2. Partially, we can recognize the solid armature at the right side and the breech end with the terminations of the power coaxial cable. A better description of the adopted setup will be provided in the final version of the paper.
The capacitor bank is charged through a 1 kΩ resistor by means of a high voltage DC generator. An optical trigger starts the discharge of the capacitor module. A photograph of the capacitor module (right side – green case), of the HVDC generator (in the center – black case) and of the 1 kΩ resistor (black cylinder on the white panel) is shown in Fig. 3. A typical current behaviour is shown in Fig. 4 and it is possible to recognize the under

damped transient before the crowbar diode plays its role determining the exponential decay. Peak current up to 100 kA can be reached with corresponding induction field of about 0.5 T inside the barrel.
Under the hypothesis of perfectly conducting indefinite bars along the *y*-direction and of constant current through the rails, a zero induction field *B* is expected outside the rails and in front of the armature. The field is constant and different from zero between the rails and behind the armature, while it varies through the armature from the constant value to zero. Indeed *B* must vanish at infinity and it must vanish everywhere to the right of the armature holding $\nabla \times B = \mu J$ i.e., $\partial B / \partial z = -\mu J$ for the defined 2D case [10]. On the other hand, the finite *y*-dimension of the rails determines a magnetic field in front of the armature where the launch mass with the possible electronics is located.

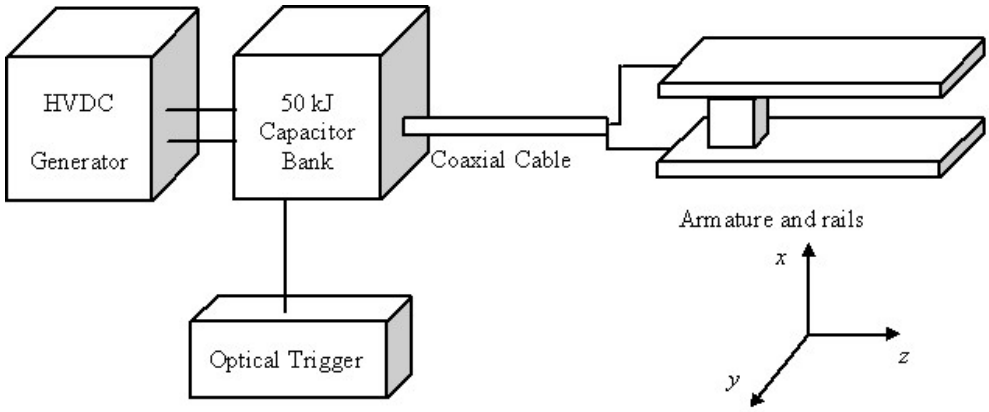

Figure 1. Schematic of the adopted experimental setup.

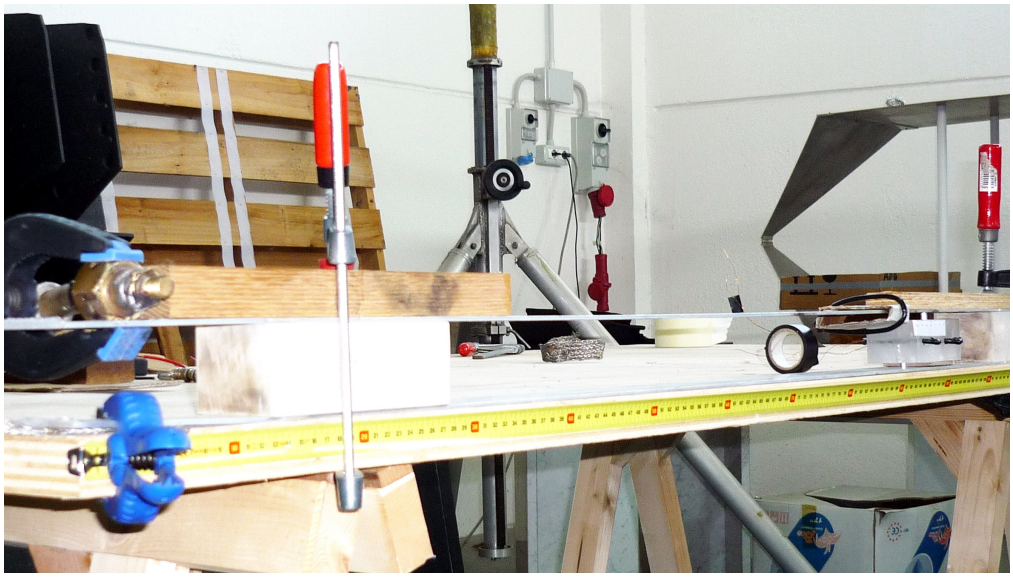

Figure 2. Photograph of the rail launcher prototype.

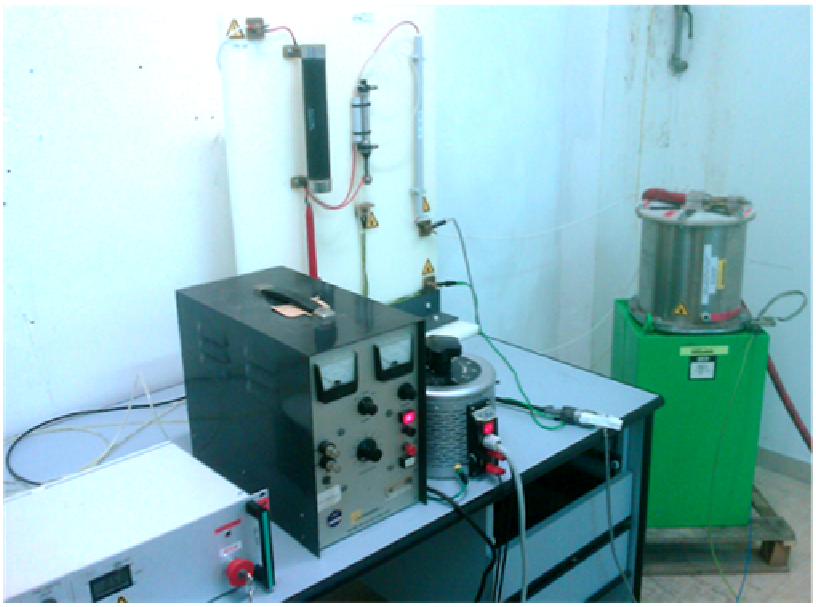

Figure3. Photograph of the capacitor module and HVDC generator. The black cylinder on the white panel is the 1 kΩ charge resitor.

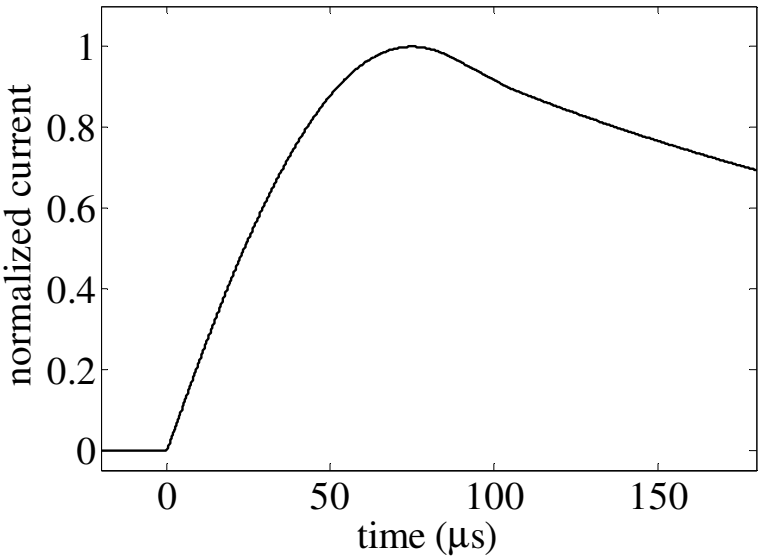

Figure 4. Typical current transient.

III. Shield Configurations and Remarks

The basic investigated shield configuration is shown in Fig.5. The shields are cylindrical shells with different geometry of the directrix (circular and square for our analysis). The front and back side of the shield are open. The geometry of the adopted shields is shown in more detail in Fig.6. Shields were made of aluminium, iron and brass with various thicknesses. For all the shields, the external diameter and edge were 30 mm. The shield length was 200 mm.

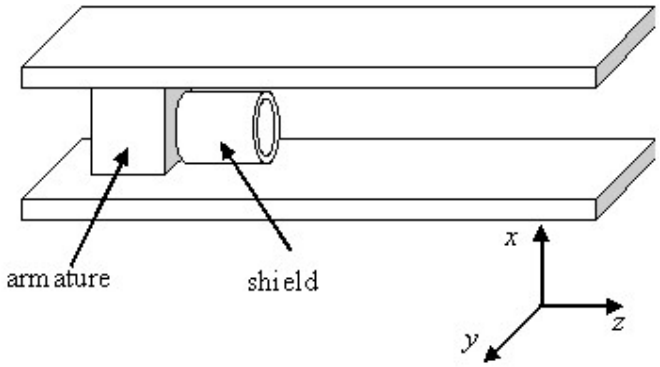

Figure 5. Schematic diagram of the rails, armature and shield.

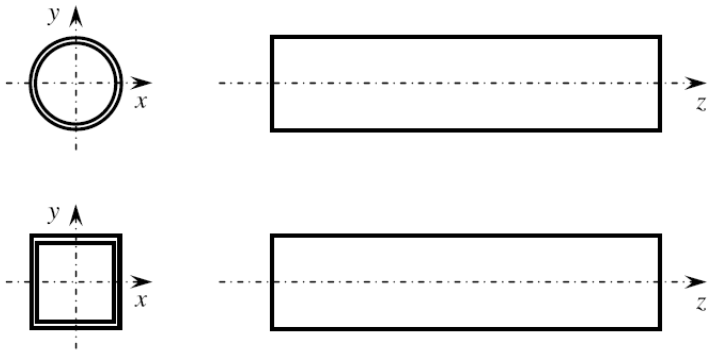

Figure 6. Geometry of the adopted shields.

The launch mass is located in the near field region and the presence of possible electrical loops in the device to be launched can be critical due to the very high magnetic fields and the transient nature of the feeding current. Our purpose is to investigate the magnetic field coupling between the rail-armature system and the electrical device in the launch mass through the use of representative measurement loops. In such a way, we evaluate the flux linked with the search loops for estimating the effective shielding performances. Thus we estimate the shielding effectiveness as the ratio between the average field without and with the shield over the region of interest.

IV. Preliminary Experimental Results

A rectangular search loop positioned on the *x-z* plane of dimensions 25 mm × 100 mm and 5 turns was adopted to test the shielding effectiveness. Measurements have been performed without and with shields. According to the theory and to the transient nature of the field, the shielding effectiveness exhibits different values at different times. The SE behaviour vs. time of the square (left plot) and circular (right plot) aluminium (solid line), brass (dotted line) and iron (dashed line) shields are reported in Fig. 7. Corresponding values at the current peak value (73 μs) and at 90 μs are summarized in Table I. Thicknesses of the shields are: circular iron 1.5 mm, square iron 1.5 mm, circular brass 2 mm, square brass 1 mm, circular aluminium 2 mm, square aluminium 3 mm.

Table I. Shielding Effectiveness (dB) at 73 μs and 90 μs.

	Circular (t = 73 μs)	Square (t = 73 μs)	Circular (t = 90 μs)	Square (t = 90 μs)
iron	16.95	36.89	18.68	36.85
brass	10.12	7.02	8.84	5.92
aluminium	14.67	> 70	13.71	> 70

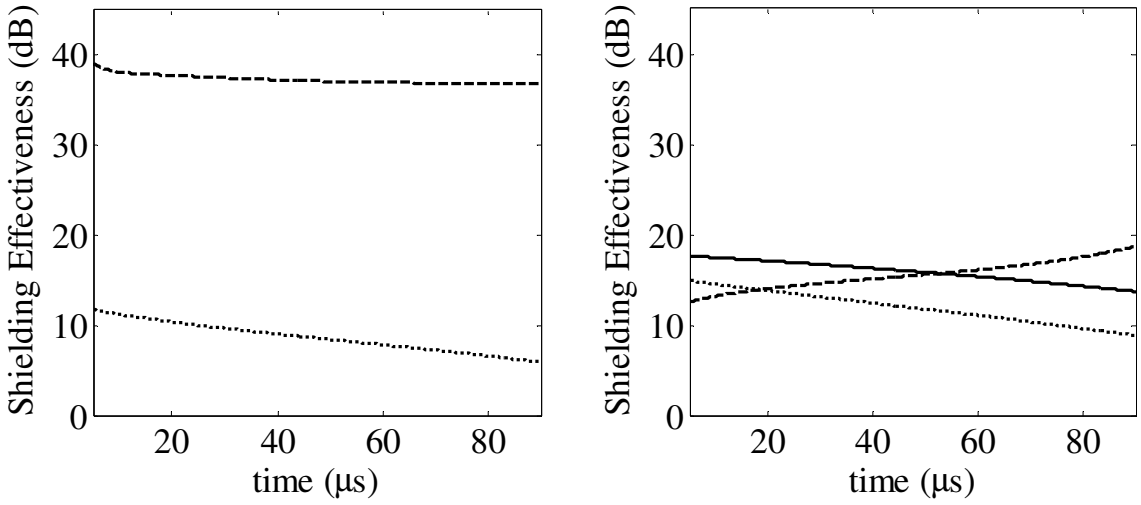

Figure 7. SE behaviour vs. time of the square (left plot) and circular (right plot) aluminium (solid line), brass (dotted line) and iron (dashed line) shields.

In Fig. 8, we show the magnetic flux obtained by the search loop vs. time without shield (dash-dotted line) and with shield (aluminium – solid line, brass – dotted line, and iron – dashed line) for the square (left plot) and circular (right plot) shields. Values are normalized with respect to the maximum value of the magnetic flux without shield.

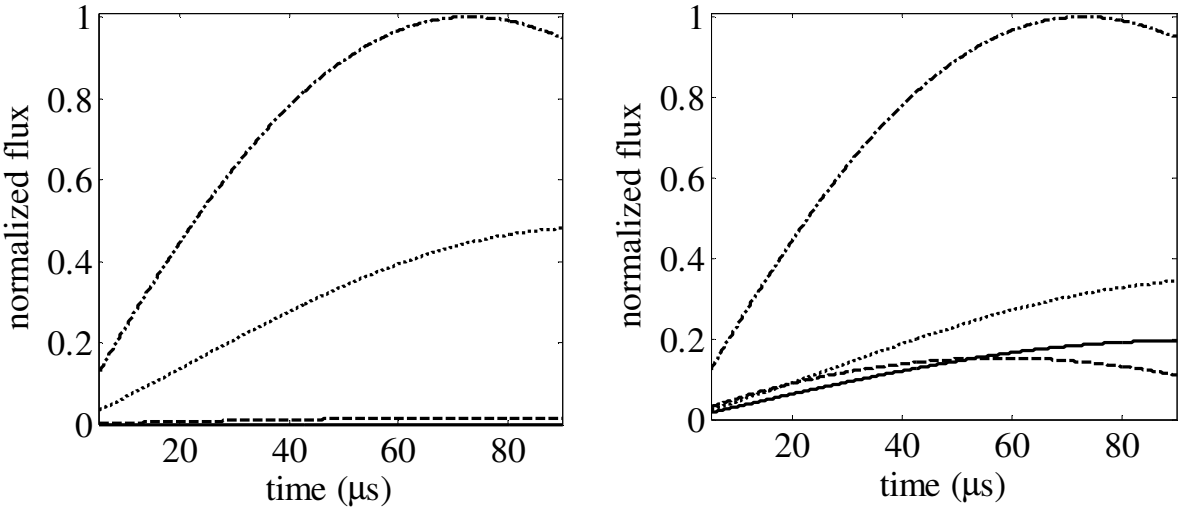

Figure 8. Normalized magnetic flux vs. time measured without shield (dash-dotted) and with shield (aluminium – solid line, brass – dotted line, and iron – dashed line) for the square (left plot) and circular (right plot) shields.

V. Conclusions

The shielding of transient high magnetic fields such as those encountered in electromagnetic rail launchers environment is an important task for correct operation of the electronics on board launch mass. In a previous study, different basic shield configurations have been investigated through a finite element analysis with discussion of main parameters. The aim of this paper was to assemble an experimental set-up and to provide preliminary results of an experimental analysis aimed at characterizing the shielding performance of cylindrical shell configurations in rail-gun bores. Experiments were performed under static conditions for single brush solid armature and for various shields.

Acknowledgments

The authors wish to thank the ISL Saint-Louis (Fr) institute, Dr. E. Spahn and Dr. M. Schneider for providing the 50 kJ unit source.

References

[1] S. A. Schelkunoff, *Electromagnetic Waves*, Princeton, NJ: Van Nostrand, 1943.
[2] J. F. Hoburg, "Principles of quasistatic magnetic shielding with cylindrical and spherical shields," *IEEE Trans. Electromagn. Compat.*, vol. 37, no. 4, pp. 574–579, Nov. 1995.
[3] S. Di Fraia, M. Marracci, B. Tellini and C. Zappacosta, "Shielding Effectiveness Measurements for Ferromagnetic Shields," *IEEE Trans. Instrum. and Meas.*, vol. 58, no. 1, pp. 115-121Jan. 2009.
[4] J. F. Hoburg, "A computational methodology and results for quasistatic multilayered magnetic shielding," *IEEE Trans. Electromagn. Compat.*, vol. 38, no. 1, pp. 92–103, Feb. 1996.
[5] P. Sergeant, M. Zucca, L. Dupré, and P. E. Roccato, "Magnetic shielding of a cylindrical shield in nonlinear hysteretic material," *IEEE Trans. Magn.*, vol. 42, no. 10, pp. 3189–3191, Oct. 2006.
[6] W. J. Biter, Magnetic shielding for high fields Contract # DAAE30-96-C-0023, Final Report, Oct. 15, 1996.
[7] Y. Trenkler and L. E. McBride, "Shielding improvement by multi-layer design," Proc. EMC Symp., Aug. 21–23, 1990, pp. 1–4.
[8] A. Zielinski, In-bore magnetic field management Army Res. Lab., Adelphi, MD, Report ARL-TR-1914, Mar. 1999.
[9] G. Becherini, S. Di Fraia, R. Ciolini, M. Schneider, B. Tellini, "Shielding of High Magnetic Fields," *IEEE Trans. Magn.*, vol. 45, no. 1, pp. 604-609, Jan. 2009.
[10] J. D. Powell and J. H. Batteh, "Plasma Dynamics of an arc-driven, electromagnetic, projectile accelerator," *J. Appl. Phys.*, vol. 52, no. 4, pp. 2717-2730, April 1981.